Structural Insights Into the Cellular Retinaldehyde-Binding Protein (CRALBP)

Tianyun Liu,[1] Ekachai Jenwitheesuk,[2] David C. Teller,[1]* and Ram Samudrala[2]*
[1]*Department of Biochemistry, University of Washington, Seattle, Washington*
[2]*Department of Microbiology, University of Washington, School of Medicine, Seattle, Washington*

ABSTRACT **Cellular retinaldehyde-binding protein (CRALBP) is an essential protein in the human visual cycle without a known three-dimensional structure. Previous studies associate retinal pathologies to specific mutations in the CRALBP protein. Here we use homology modeling and molecular dynamics methods to investigate the structural mechanisms by which CRALBP functions in the visual cycle. We have constructed two conformations of CRALBP representing two states in the process of ligand association and dissociation. Notably, our homology models map the pathology-associated mutations either directly in or adjacent to the putative ligand-binding cavity. Furthermore, six novel residues have been identified to be crucial for the hinge movement of the lipid-exchange loop in CRALBP. We conclude that the binding and release of retinoid involve large conformational changes in the lipid-exchange loop at the entrance of the ligand-binding cavity. Proteins 2005;61:412–422.** © **2005 Wiley-Liss, Inc.**

Key words: cellular retinaldehyde-binding protein; homology modeling; molecular dynamics; ligand-binding cavity; lipid-exchange loop

INTRODUCTION

Cellular retinaldehyde binding protein (CRALBP) is a water-soluble protein found in the retina and pineal gland that carries 11-*cis*-retinal or 11-*cis*-retinol as endogenous ligands.[1] Mouse knockout studies have shown that CRALBP gene defects impair regeneration of visual pigments.[2] CRALBP functions in retinal pigment epithelium (RPE) as a major acceptor of 11-*cis*-retinol in the isomerization step of the rod visual cycle. It also serves as a substrate carrier for 11-*cis*-retinol dehydrogenase (RDH5), facilitating the oxidation of 11-*cis*-retinol to 11-*cis*-retinal.[2–6] CRALBP has been found to interact with 11-*cis*-retinol dehydrogenase and with ERM (ezrin, radixin, moesin)-binding phosphoprotein 50 (EBP50).[7] The interaction between CRALBP and EBP50 in RPE suggests a mechanism for localizing CRALBP to RPE plasma membrane for export of 11-*cis*-retinal to the adjacent rod photoreceptor cells for visual pigment regeneration.[7,8]

Ten different mutations within the human gene encoding CRALBP (RLBP1) have been reported, including six missense (G145D, R150Q, R150W, I200T, M225K, and R233W), two frame-shift, and two splice-site alterations.[9–14] The missense mutations are associated with retinal pathologies such as autosomal recessive retinitis pigmentosa (RP), Bothnia dystrophy (BD), retinitis punctata albescens (RPA), and Newfoundland rod–cone dystrophy (NFRCD). Biochemical studies have shown that these mutations can either enhance or abolish CRALBP–retinoid interactions.[9–14] However, the molecular basis for the pathology as a result of impaired CRALBP function is not well understood due to lack of structural data.

Substantial efforts have been made to characterize CRALBP–ligand interactions and the structure of the retinoid binding pocket.[4,15–17] Mutagenesis studies have implicated 10 residues as potentially interacting with retinoid, including W165, Y179, F197, C198, M208, Q210, M222, V223, M225, and W244.

Based on sequence information, CRALBP has been classified as a member of the CRAL-TRIO lipid-binding protein family (Pfam entry: PF00650).[18] Crystal structures have been determined for three CRAL-TRIO lipid-binding proteins: human α-tocopherol transfer protein (ATTP),[19,20] yeast Sec14,[21] a phosphatidylinositol-binding protein, and human supernatant protein factor (SPF).[22]

The lipid-exchange loop region in the CRAL-TRIO family is strongly conserved in CRALBP residues 241–264[17,18]; it forms a helical conformation in Sec14, SPF, and ATTP.[19–22] Recent NMR studies suggest that conformational changes of the lipid-exchange loop in CRALBP are important for ligand association and dissociation.[16,17] Interestingly, two conformation types of this lipid-exchange loop have been identified in crystal structures of CRAL-TRIO family members.[19–22] For example, the crystal structures for ATTP have been determined in a closed "carrier" conformation and an open "membrane-docking"

Grant sponsor: Searle Scholar Award (to R. Samudrala). Grant sponsor: National Science Foundation; Grant number: DBI-0217241 (to R. Samudrala). Grant sponsor: National Institutes of Health; Grant numbers: GM068152 (to R. Samudrala) and GM63020 (to D. C. Teller). Grant sponsor: U.S. PHS; Grant numbers: EY01730, EY08061, and EY0861 (to D. C. Teller).

Correspondence to: Ram Samudrala, Department of Microbiology, University of Washington School of Medicine, Seattle, WA 98195. E-mail: ram@compbio.washington.edu. David C. Teller, Department of Biochemistry, University of Washington School of Medicine, Seattle, WA 98195. E-mail: teller@u.washington.edu

Received 30 November 2004; Revised 14 March 2005; Accepted 14 April 2005

Published online 24 August 2005 in Wiley InterScience (www.interscience.wiley.com). DOI: 10.1002/prot.20621

conformation.[19,20] The difference between the two crystal forms occurs in the lipid-exchange loop (residues 198–221). The conformation states of this segment affect ligand access to the ligand-binding cavity.[19,20]

To elucidate the functional mechanism of CRALBP, we generated structural models of the protein using homology modeling and molecular dynamics (MD) simulations. The homology models were constructed by mixing and modeling the templates generated from the four available crystal structures of the CRAL-TRIO lipid-binding proteins. Using these models, we provide structural insights into the possible functional effects of pathology-associated mutations. The models of CRALBP indicate two possible conformations, with the lipid-exchange loop either in the open or the closed forms. By analyzing the MD simulation trajectories of the open and the closed forms of CRALBP, we assign distinct functions to these conformations. We hypothesized that the movement of this loop is regulated by its hinge region, and investigated the possible effect of mutations in these regions.

MATERIALS AND METHODS

Structural Modeling

The sequence alignment of CRALBP, ATTP, SPF, and Sec14 presented by Hendrickson and coworkers[20] was used to generate structural superposition in selected regions (CRALBP residues 66–294) using in-house software.[17] Residues for equivalence were selected if the distance was within 2.5 Å. This value was determined by comparing trials with different cutoffs. Using this cutoff, the structures typically matched well within the aligned regions.

The crystal structures of ATTP, SPF, and Sec14 were obtained from the Protein Data Bank (PDB entry: 1AUA for Sec14,[21] 1O6U for SPF,[22] 1R5L for ATTP,[20] and 1OIZ for ATTP[19]). They consist of two types of conformations, with the major differences occurring in the lipid-exchange loop. 1AUA (Sec14) and 1OIZ (ATTP) have open lipid-exchange loops, whereas 1O6U (SPF) and 1R5L (ATTP) have closed loops. Both closed forms, 1O6U (SPF) and 1R5L (ATTP), were crystallized with their physical ligands, α-tocopherylsquinone and α-tocopherol, respectively. The open forms, 1AUA (Sec14) and 1OIZ (ATTP), were crystallized in the presence of detergent or additive molecules, which occupy the ligand-binding cavity where they replace the physical ligands.

Based on each individual template, initial models of CRALBP were built using programs in the RAMP software suite[23,24] including `scgen_mutate`, `mcgen_exhaustive`, `mcgen_semfold_loop` and `potential`, with side-chain conformations rebuilt using the SCWRL3 program.[25] Initial models were then divided into two groups according to the conformation of their lipid-exchange loop. Thus, two possible conformations of CRALBP were generated by mixing and matching initial conformations within each group to reach an optimal combination of the main-chain and side-chain possibilities. This step was achieved with the program `cf` from RAMP, which utilizes an algorithm based on graph theory to handle the context–sensitivity of interactions in protein structures.[23,24] Final models were energy-minimized using ENCAD.[26]

TABLE I. Results of Protein Structure Check by PROCHECK

	Closed conformation	Open conformation
Residues in most favored regions	178 (86.4%)	177 (85.9%)
Residues in additional allowed regions	22 (10.7%)	26 (12.6%)
Residues in generously allowed regions	2 (1.0%)	1 (0.5%)
Residues in disallowed regions	4 (1.9%)	2 (1.0%)
Number of non-Gly and non-Pro residues	206 (100.0%)	206 (100.0%)
Number of end residues	2	2
Number of Gly residues (shown in while boxes)	13	13
Number of Pro residues	8	8
Total number of residues	229	229
Overall PROCHECK score*	0.03	0.04

*Recommended value > -0.50 and investigation is needed for < -1.0.

The CRALBP models were constructed in the ligand-bound form. The retinal Schiff base was taken from the rhodopsin coordinates (PDB entry: 1HZX) and converted to 11-*cis*-retinal. The 11-*cis*-retinal was oriented in models by trials such that after energy minimization, the aldehyde group was solvent-inaccessible.[5,15] The position of 11-*cis*-retinal within the ligand-binding cavity of the CRALBP closed conformation was determined by multiple energy minimizations and dynamics calculations using NAMD[27] with the CHARMm22 force field.[28,29] The coordinates of the 11-*cis*-retinal in the closed conformation were copied to the open conformation to set the initial ligand position for further simulation.

To validate our CRALBP models, Ramachandran plots were created and the structures were analyzed by PROCHECK (Table I).[30] The model figures were prepared with MOLSCRIPT[31] and Raster3D.[32]

Generation of CRALBP Mutant Structures

The structures of CRALBP mutants were generated using SCWRL3, which is a program for adding side-chains to a protein backbone based on a backbone-dependent rotamer library.[25] They were categorized into two groups. In the first group, structures of CRALBP missense mutants, which have been identified clinically and experimentally to have effects upon ligand binding[4,15–17] (Table II), were created using the CRALBP wild-type closed form structure. These mutants are G145D, R150Q, R150W, W165F, Y179A, F197A, C198A, I200T, M208A, Q210R, M222A, V223A, M225A, M225K, R233W, and W244F.

To investigate the mechanism of lipid-exchange loop movement, a second group of mutations were created in silico using the CRALBP wild-type structure: Q242R, P243A, W244A, W244F, K254A, K254Q, P255A, F256A, L257P, E263D, R264A, and V265A. For these mutants, structures of both the open and the closed forms were generated based on the corresponding parent CRALBP structures.

TABLE II. Equilibrium Dissociation Constant (*Kd*) of CRALBP With 11-*cis*-Retinal and Interaction Energies Calculated From MD Trajectories

CRALBP	Binding affinity to *11-cis-retinal*	$E_{(wt)}^{vdw}$ (kcal/mol)	$E_{(M)}^{vdw}$ (kcal/mol)	$E_{(WT)}^{elec}$ (kcal/mol)	$E_{(M)}^{elec}$ (kcal/mol)	ΔE^{inter} (kcal/mol)	Predicted roles
A. Pathogenic mutations of CRALBP identified clinically							
R233W	$Kd_{(M)}/Kd_{(WT)}$: 0.5	−0.0051	−0.1429	0.6203	0.5997	0.1585	IR
M225K	ARB	−3.3004	−4.1633	0.2674	0.7248	0.4054	IR
R150Q	ARB	0.0	0.0	0.0	0.0	0.0	SC
R150W	ARB	0.0	0.0	0.0	0.0	0.0	SC
G145D	Unknown	−0.0026	0.0033	1.8217	0.0798	1.7413	SC
I200T	Unknown	−0.3142	−0.0925	−2.1645	0.2557	−2.6419	SC
B. Residues as components of the CRALBP ligand-binding cavity identified experimentally							
M225A	$Kd_{(M)}/Kd_{(WT)}$: 2.6	−3.3004	−0.8240	0.2674	0.2520	−2.4911	IR
M222A	$Kd_{(M)}/Kd_{(WT)}$: 2.5	−2.1510	−0.0477	−0.0373	0.4421	−2.5826	IR
Q210R	$Kd_{(M)}/Kd_{(WT)}$: 1.6	0.0013	−0.1153	0.0777	0.7454	−0.5511	EL
W165F	ARB	−3.3226	−0.0236	−1.1620	−0.2872	−4.1738	IR
W244F	$Kd_{(M)}/Kd_{(WT)}$: 2.0	0.0	0.0	0.0	0.0	0.0	CL
M208A	$Kd_{(M)}/Kd_{(WT)}$: 2.0	0.0	0.0	0.0	0.0	0.0	EL
Y179A	Unknown	−2.5577	−0.0220	2.8715	0.4205	−0.0847	IR
F197A	Unknown	−0.0558	−0.0123	0.2587	0.2334	−0.0182	IR
C198A	Unknown	−0.0720	−0.0480	0.1235	0.1519	−0.0523	SC
V223A	Unknown	−0.0051	−0.1938	0.1235	0.4459	−0.1336	SC

Interaction energies (kcal/mol) calculated on MD simulation trajectories starting from 900 ps to 1 ns are averaged. It includes two parts, electrostatic (E^{elec}) and van der Waals (E^{vdw}) interaction energies. The difference of interaction energies between the wild-type CRALBP and mutants are calculated as $(E_{(WT)}^{vdw} + E_{(WT)}^{elec}) - (E_{(M)}^{vdw} + E_{(M)}^{elec})$, referred as ΔE^{inter}. The interaction energy is set to zero when the average distance between a residue and 11-*cis*-retinal is larger than 12Å. $Kd_{(M)}/Kd_{(WT)}$ indicates the ratio between *Kd* of mutant and *Kd* of wild type CRALBP.[4,15–17] When individual residues are mutated as shown in the table, the changes of interaction energies between the corresponding residue and 11-*cis*-retinal are correlated with the changes of *Kd* accordingly. Possible roles of each residue are also predicted based on the CRALBP models (Fig. 2).

ARB, abolishment of retinoid binding;
IR, interaction with retinoid;
SC, stabilization of the core βαβαβαβ fold;
EL, entrance of the ligand-binding cavity;
CL, component of the lipid-exchange loop.

Molecular Dynamics Simulations

All MD simulations were performed using the NAMD package version 2.5[27] with CHARMm22 force field.[28,29] The van der Waals, bond, angle, dihedral, and improper dihedral parameters in X-PLOR format[33] for the noncovalent bonded retinal were adopted from the Hetero-Compound Information Centre–Uppsala (HIC-Up)[34] and modified to the CHARMm22 format according to the parameter and topology files for Schiff base–linked retinal provided in the "ParameterTopologyRepository."[35] The parameter and topology files were validated by trials of MD simulations and visual observations of 11-*cis*-retinal movements in visual molecular dynamics (VMD).[36]

The protein–ligand complexes were immersed in a 20-Å-radius sphere of transferable intermolecular potential (TIP3)-water using the program SOLVATE[37] to allow the protein–ligand complexes to relax in an aqueous environment. Sodium and chloride ions were added at isotonic (physiological) concentration 0.154 mol/L obeying the Debye–Hückel distribution. The system was then energy-minimized for 1000 steps in a conjugate gradient scheme.

The MD simulations were performed using the standard protocol and default settings provided by the NAMD package. The system was heated up gradually from 0 K to 300 K in 24 picoseconds (ps), followed by a 20 ps equilibration with the backbone protein atoms constrained, and 1 nanosecond (ns) equilibration without constraints. The temperature was kept at 300 K by applying Langevin forces for velocity rescaling every 20 ps. The integration timestep was 1 femtosecond (fs). The equilibration was performed in the NpT ensemble using the Nosé–Hoover Langevin piston pressure control.[38] The nonbonded interactions were calculated using a smooth (10–12 Å) cutoff. The trajectories were recorded every 1 ps. The simulations were repeated with three different starting seeds. The wild-type CRALBP conformation and its mutant structures were subjected to the same simulation protocol.

Analysis of Molecular Dynamics Simulation Trajectories

For the first group of CRALBP missense mutants, the average interaction (electrostatics and van der Waals) energies between 11-*cis*-retinal and residues in the mutant structures (Table II) were calculated. These energies were obtained from MD simulation trajectories using the NAMD Tools package by averaging over the individual interaction energies for 100 structures recorded at 1 ps intervals from 900 ps to 1 ns. The standard errors for the

Fig. 1. Sequence alignment of four CRAL-TRIO proteins. Wild-type residues of retina pathogenic mutants that have been identified clinically are highlighted in pink. Residues mapped by biochemical methods to be involved in protein–ligand interactions are highlighted in blue. Identical residues are indicated in green, and similar residues are indicated in yellow. Residues in the lipid-exchange loop of CRALBP are boxed. Gray regions were not used for homology modeling.

average interaction energies were all extremely small and are not included in Table II.

To analyze the second group of mutants, structures extracted from MD simulation trajectories were superimposed on the starting CRALBP structure using the `fit` and `rmsd` programs in the RAMP software suite.[23] All α-carbon root-mean-square deviation (cRMSD) calculations were performed after superposition.

RESULTS AND DISCUSSION

Structural Models of CRALBP

Previously, we generated a structural model of the CRALBP ligand-binding cavity using a crystallography refinement method combined with homology modeling.[17] In this work, we extend the modeling region to the N-terminal domain of CRALBP, which facilitates the correct folding of the ligand-binding cavity domain. Moreover, using an improved homology modeling method with an algorithm based on graph theory,[24] this new model provides more accurate structural insights into CRALBP.

Structure modeling programs in RAMP use the conditional probabilities of pairwise atom–atom distances from proteins with known structures and a hybrid Monte Carlo/genetic algorithm minimization protocol to predict native-like protein conformations.[23] The method used in this study is different from general homology modeling procedures. It utilizes an algorithm based on graph theory to handle the context–sensitivity of interactions in protein structures in order to obtain a most probable three-dimensional (3D) structure of a protein.[24] The advantage of this method is that information from multiple parent conformations can be mixed and matched to reach an optimal combination of the main-chain and side-chain candidates. This has been shown to be effective in blind prediction of protein structures as evaluated in the sixth Critical Assessment of Protein Structure Prediction methods experiment.

CRALBP shares 20–33% sequence identity with conserved regions of the three CRAL-TRIO family members (ATTP, SPF, and Sec14). The alignment between them spans 229 amino acids (CRALBP: residue Q66 to residue K294) and includes their respective ligand-binding pockets[18] (Fig. 1). According to our alignment, the CRAL-TRIO ligand-binding domain in CRALBP starts from residue R120 and ends approximately at residue K294.

The structure of CRALBP consists of two domains, an N-terminal all-helical domain and a C-terminal domain, which at its core is composed of a βαβαβαβ fold. The N-terminal domain of CRALBP (residues 66–119) is partially modeled (Fig. 2); it consists of 4 α-helices, which are arranged essentially antiparallel to each other. The first three helices form a tripod-like motif, and the last helix links the N-terminal domain and the C-terminal domain tightly. As the core of the C-terminal domain, the ligand-binding cavity contains a parallel β-sheet as the floor of the cavity, with two α-helices forming one side of the cavity, and one helix and its connecting loop covering the entrance (Fig. 2).

The lipid-exchange loop (CRALBP 241–264) is conserved among the CRAL-TRIO family members, including CRALBP, Sec14, SPF, and ATTP.[19–22] The existence of two distinct conformations, the open and the closed forms, suggests two different functional states in ligand binding of this protein family.[17] Accordingly, we have generated two models in which the lipid-exchange loops are in the open and the closed forms, respectively. In our model, the closed conformation of this "lipid-exchange loop" forms an α-helix. The open form also shows helical conformation with local distortions. However, the helix rotates away from the center β-sheet of the ligand-binding cavity, opening up the cavity and thereby exposing an extended hydrophobic patch comprised of residues F246, V252, V253, F256, L257, L261, and L262 to the solvent side. In the closed form, these residues face the inside of the ligand-binding cavity (Fig. 2).

Since CRALBP binds 11-*cis*-retinal with higher affinity than any other retinoid,[1] we first manually docked 11-*cis*-retinal as its ligand in the model of CRALBP. In the closed conformation, the final position of 11-*cis*-retinal in the ligand cavity has been optimized by multiple energy

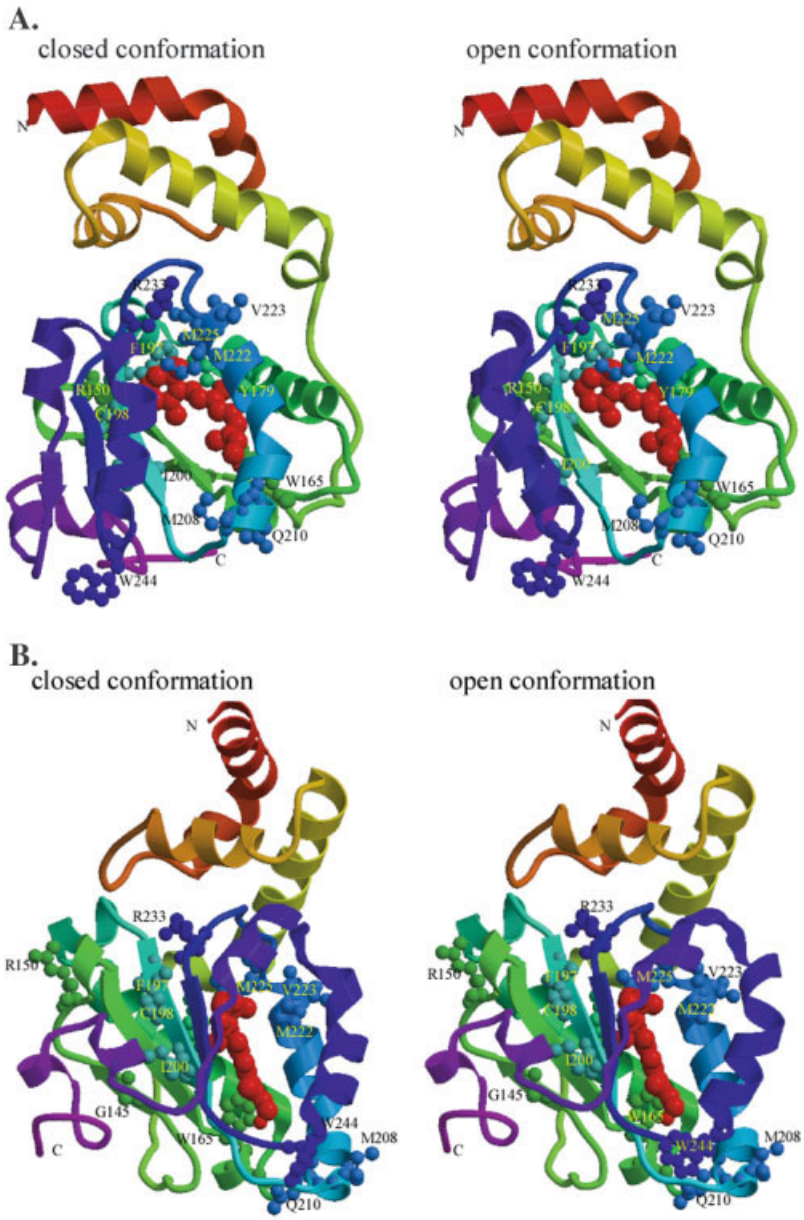

Fig. 2. Structural models of CRALBP in open and closed conformations. Open and closed conformations are shown in two different views: (**A**) viewed from the entrance of the ligand-binding cavity, and (**B**) a 60° rotation from the view in (A). The backbone ribbon is rainbow-colored from red at the N-terminal Q66 to violet at the C-terminal K294. The lipid-exchange loop is indicated in dark blue. Five residues associated with retinal pathology and nine residues implicated in protein–ligand interactions by biochemical experiments are drawn in ball and stick configuration. The ligand 11-*cis*-retinal is colored in red. Images were prepared using MOLSCRIPT[31] and Raster3D.[32]

minimization and MD simulations. After MD simulations, the ligand stays inside the cavity and the aldehyde group is solvent-inaccessible.[5,15] In our model for the CRALBP closed form, the ionone ring points toward residues M222 and M225, and interacts with residues Y179 and Y197. The aldehyde group forms a hydrogen bond with the free amino group of residue R218. Residue W165 is very close to the aldehyde group of 11-*cis*-retinal, suggesting a possible interaction with retinoid (Fig. 2). Residues W165, Y179, Y197, M222, and M225 have been implicated biochemically to associate with the CRALBP ligand-binding cavity.[4,15–17] This further supports the reliability of the placement of ligand. The size of ligand-binding cavity is relatively large for 11-*cis*-retinal, which suggests that water molecules may be involved in protein–ligand interactions.

In previous crystallography experiments,[19–22] the closed conformation of the CRAL-TRIO proteins is only observed with the physical ligand bound. The open conformation is observed in presence of detergent or additive molecules,

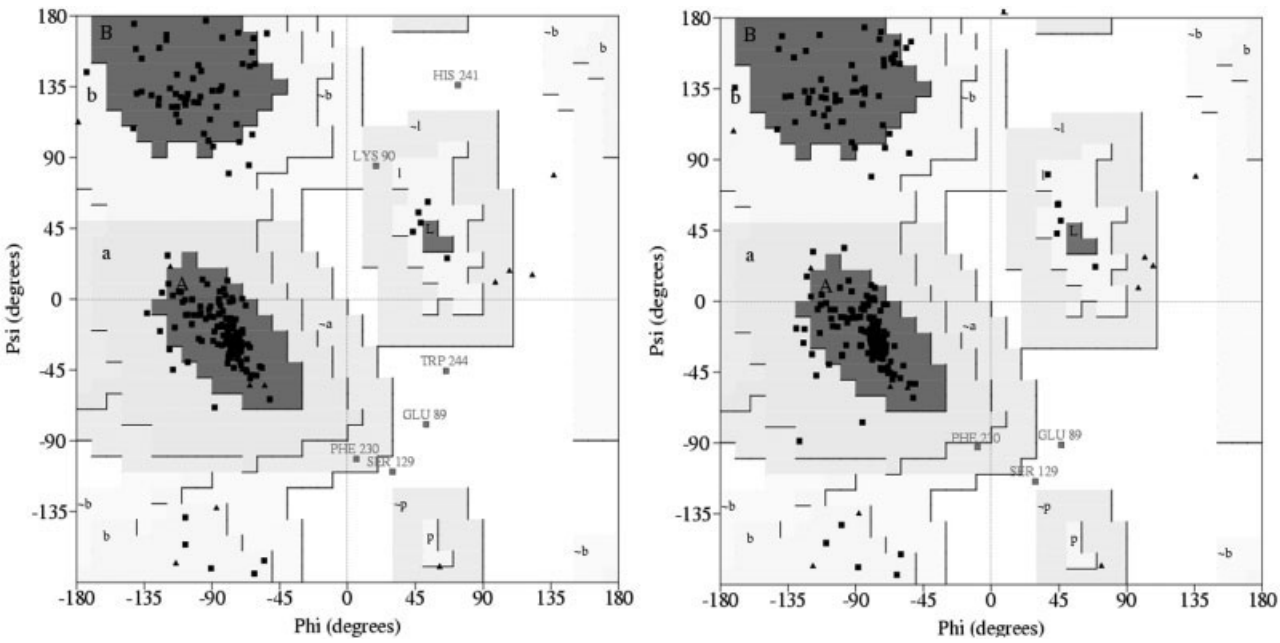

Fig. 3. Ramachandran plot of the homology-modeled structures of CRALBP in both the closed (left) and open (right) conformations.

which stabilize the conformation. A conformation of the CRAL-TRIO lipid binding protein with an empty ligand-binding cavity has not been observed in either the open or the closed form. However, in the MD calculations of the open conformation, the retinal shows a tendency to dissociate from the ligand-binding cavity. Therefore the initial coordinates of the 11-*cis*-retinal in the CRALBP open conformation are based on the position of the ligand in the closed form.

Ramachandran analysis suggests that our models are reasonable with respect to the overall fold (Fig. 3 and Table I). Both the open and the closed conformations of CRALBP have been deposited in the PDB as 1XGG and 1XGH, respectively.

Mapping of Pathology-Associated Mutations on the CRALBP Closed Conformation and Identification of Residues in the CRALBP Ligand-Binding Cavity

Clinical studies have associated six missense mutations within the human CRALBP gene with recessive progressive retinopathy.[9–14] They are G145D, R150Q, R150W, I200T, M225K, and R233W. Biochemical experiments have shown that these mutations can either enhance or abolish retinoid binding leading to retinal pathologies.[4,15–17]

Our CRALBP models map the pathology-associated mutations either directly in or adjacent to the ligand-binding pocket (Fig. 2). Residue M225 shows a close contact with 11-*cis*-retinal, forming a hydrophobic interaction with the ionone ring. From MD simulation trajectories, we calculate the interaction energy between 11-*cis*-retinal and residue M225, and its counterpart residue in mutant structure K225, respectively [Table II(A)]. The substitution of residue M225 by lysine maintains the van der Waals contact through the partial hydrophobic side-chain of lysine. However, it introduces positive charges that result in the instability of the hydrophobic core of the ligand-binding cavity, thus leading to the abolishment of retinoid binding to CRALBP.[4] On the other hand, substitution of residue M225 by alanine shows an energy preference ($\Delta E^{\text{inter}} = -2.49$ kcal/mol) [Table II(B)], indicating that it may enhance the retinoid binding to CRALBP. Residues I200 and G145 co-locate in the core β-sheet that forms the floor of the ligand-binding cavity (Fig. 2). Mutations I200T and G145D may destroy the continuity of the β-sheet.

Residue R150 is distant from the ligand-binding cavity in our model (Fig. 2). In our interaction energy calculation, the average distance between residue R150 and 11-*cis*-retinal is beyond the threshold of 12 Å. The interaction energy between them is set to zero. Residue R150 interacts with residue E191 in the core βαβαβαβ structure, and contributes to the stabilization of the βαβαβαβ fold. Mutation R150Q or R150W may destroy this essential contact, resulting in the destabilization of the hydrophobic pocket, leading to the abolishment of retinoid binding.[10,14] As a component of the ligand-binding cavity, the side-chain of residue R233 is in relatively close proximity to the ionic ring of 11-*cis*-retinal (Fig. 2). Substitution of residue R233 by tryptophan introduces an aromatic ring, which contributes to the stabilization of the ionone ring of retinoid. This is consistent with the observation that this mutation of CRALBP shows an increased affinity to retinoid.[5,11]

Among the 10 residues biochemically implicated in protein–ligand interactions[4,15–17] [Table II(B)], we associate seven with the ligand-binding cavity from a structural point of view (Fig. 2). Residues Y197, Y179, M222, M225, and W165 interact with 11-*cis*-retinal directly, while resi-

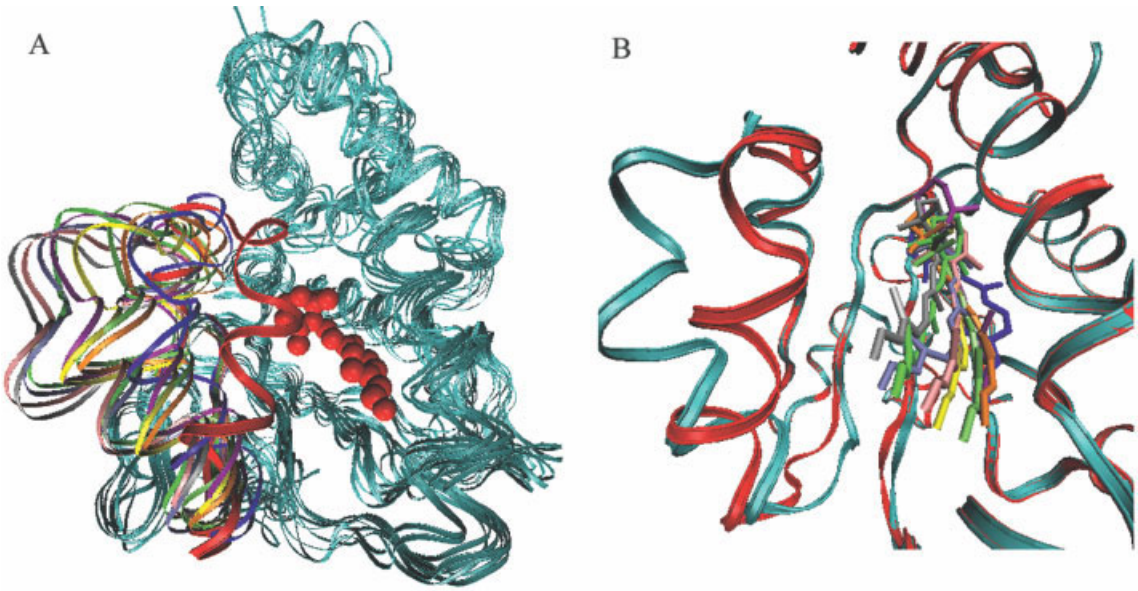

Figure 4.

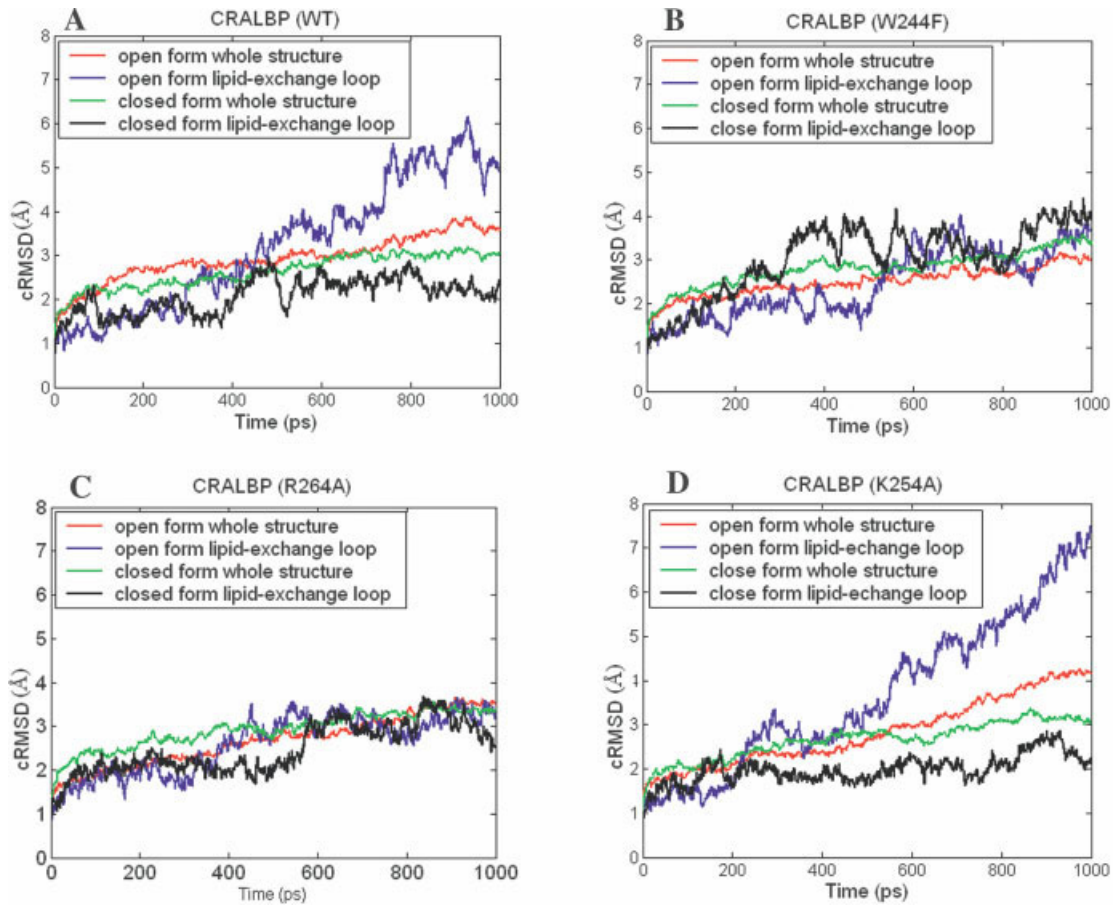

Figure 5.

dues C198 and V223 co-locate in the core β-sheet of the ligand-binding cavity. In our model, residues M208, Q210, and W244 are not involved in direct interactions with 11-*cis*-retinal; rather, they all align at the entrance of the ligand-binding cavity, controlling the opening and the closing of the cavity. We also note that residue W244 is a component of the lipid-exchange loop. The binding properties of the other eight mutations built experimentally are listed in Table II(A). The interaction energies between individual residues and 11-*cis*-retinal are also indicated. Substitutions of residue side-chains result in an increase of interaction energy, suggesting negative effects upon ligand binding. The energy calculation is in approximate agreement with experimental findings.[4,15–17]

Dynamic Properties of the Open and Closed Conformations of CRALBP

One of the conserved regions in the CRAL-TRIO family is the lipid-exchange loop.[17] Two distinct conformations of this region have been found in crystal structures.[19–22] The crystal structures of ATTP have been determined in both the open and the closed forms. The structure of Sec14 shows an open form,[21] while SPF[22] shows its closed form. Theoretically, the two forms are in an equilibrium that is shifted toward the closed form upon ligand binding. Although both the open and closed forms are stable conformations in the crystallographic structures, they represent two stable states in a dynamic process where the ligand binds to and releases from the protein. However, an open conformation of the CRAL-TRIO protein without a ligand, or ligand-like molecule binding, is not stable. This has also been suggested in our simulation trials: Simulations of the CRALBP open conformation without a ligand cannot be continued due to its large cavity. To initiate an effective MD simulation, the open conformation has been constructed in a ligand-bound form.

Since the ligand association and dissociation is a dynamic process, MD simulations could help the ligand to adopt its own position. We observed that the ligand 11-*cis*-retinal shows a tendency to dissociate from CRALBP in the open conformation simulation (Fig. 4), while staying bound in the simulation of the closed conformation.

Through MD simulations we have also observed the mobility potential of the lipid-exchange loop when it is in its open conformation, and the static properties when it is in its closed conformation (Fig. 5). The simulation trajectories and the ligand topology and parameter files may be downloaded at http://data.compbio.washington.edu/misc/downloads/cralbp/.

The structures of both the open and the closed conformations are stable and suitable for MD simulations. After the 1 ns equilibration, the cRMSD from the starting structure of the open and the closed forms reach 3.8 Å and 3.0 Å, respectively (Fig. 5). To determine the region of CRALBP that contributes most to this difference, cRMSDs of each segment have been computed separately and compared between the open and the closed forms. The "mobile lipid-exchange loop" of the open form CRALBP structure (residues 241–264) contributes most to the flexibility, with a cRMSD of 6.0 Å at 1 ns relative to the starting structure. In contrast, the cRMSD of this segment from the closed conformation stays consistently smaller (~3.0 Å) than the cRMSD of the whole structure (Fig. 5).

We monitored the movements of the lipid-exchange loop from the CRALBP open conformation (Fig. 4). During 1 ns MD simulations, this segment moves away from, and then back into, the ligand-binding cavity several times (Fig. 4). This process involves rigid body movements and local distortions in its helical conformation. Along the movements of the lipid-exchange loop, the aldehyde group of 11-*cis*-retinal moves toward the solvent, but the ionone ring of it stays its original position, interacting with residues Y179 and Y197.

A simulation time of 1 ns is too short to observe the opening of lipid-exchange loop from its closed form, or its closing from the open form. The lipid-exchange loop in the open conformation exhibits significantly greater conformational fluctuation than that in the closed form. The fact that we could not observe the transition between the open and the closed conformations also suggests that there is an

Fig. 4. Movement of the lipid-exchange loop and the ligand during MD simulations. (**A**) illustrates the rigid body movements and local distortions of the lipid-exchange loop in the open conformation of CRALBP during 1 ns simulations. Nine representative conformations are selected from MD simulations snapshots according to their cRMSDs with respect to the starting structure. After superposition on the starting structure, the backbone of the starting structure is colored in cyan and the ligand is colored in red. The lipid-exchange loop from the starting CRALBP structure in the closed conformation is also colored in red. The lipid-exchange loops from different representative conformations are colored as follows: blue (0 ps), orange (358 ps), lime (422 ps), purple (558 ps), yellow (620 ps), pink (761 ps), ice-blue (810 ps), silver (930 ps), and green (991 ps). (**B**) illustrates the movements of 11-*cis*-retinal in the open conformation of CRALBP during 1 ns simulations, with structures selected as described in Fig. 4(A). The backbones of the open and the closed conformations are colored in cyan and red, respectively. The 11-*cis*-retinal from different representative conformations are colored as follows: blue (0 ps), orange (358 ps), lime (422 ps), purple (558 ps), yellow (620 ps), pink (761 ps), ice-blue (810 ps), sliver (930 ps), and green (991 ps). The two images illustrate that in the open conformation, the lipid-exchange loop undergoes a dynamic process, which results in the transient unwinding of the lipid exchange loop, thus allowing the ligand binding. The ligand, 11-*cis*-retinal, shows the trend to dissociate from CRALBP in the open conformation simulation.

Fig. 5. Movement of the CRALBP conformations and the lipid-exchange loop as measured by cRMSD relative to the starting structures during 1 ns MD simulations. The movement of the whole structure in the open form is shown in red, and the movement of the lipid-exchange loop in the open form is shown in blue. The movement of the whole structure in the closed form is shown in black, and the movement of the lipid-exchange loop in the closed form is shown in green. All cRMSDs are calculated every 1 ps after superimposition on the backbone of the starting structures. In the wild-type CRALBP simulations (**A**), the open and the closed conformations show different flexibility, with cRMSDs of 3.8 Å and 3.0 Å, respectively. The lipid-exchange loop of the open conformation contributes most to the movement, with a cRMSD of 6.0 Å. In the simulations of mutants W244F (**B**) and R264A (**C**), the lipid-exchange loop of the open conformation shows restrained flexibility. On the other hand, in the simulations of mutant K254A (**D**), the lipid-exchange loop of the open conformation shows increased flexibility. This indicates that specific mutations in the lipid-exchange loop cause changes in its flexibility.

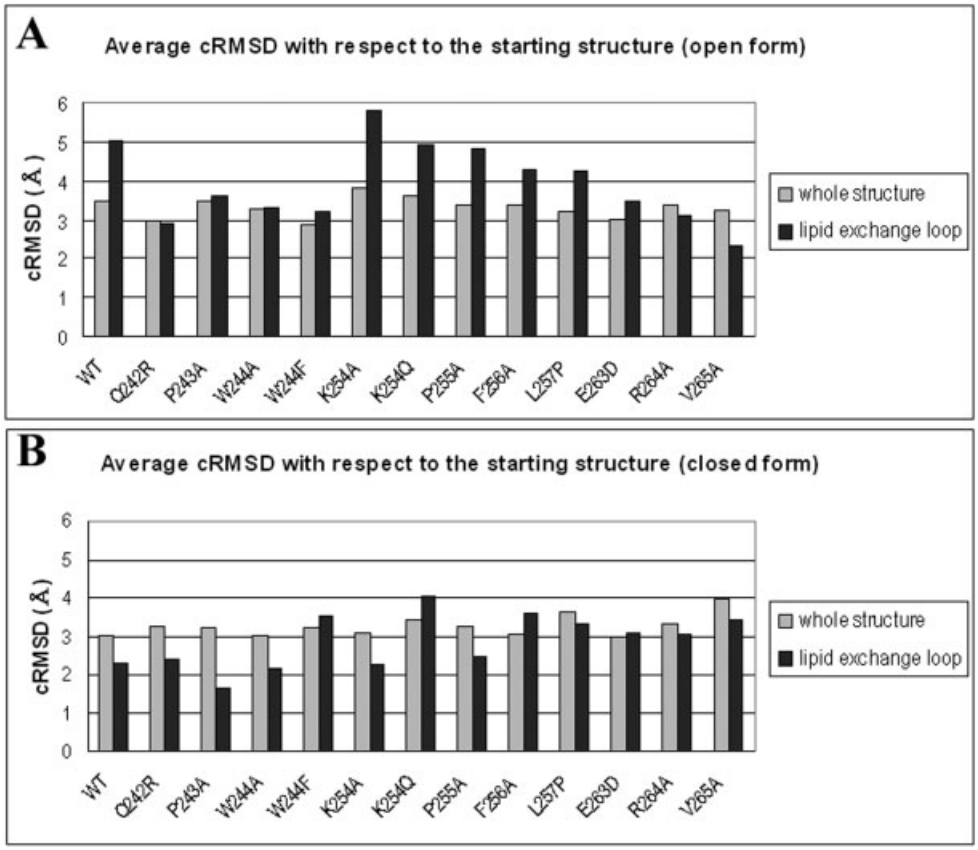

Fig. 6. Effects of point mutations in the lipid-exchange loop on its dynamics measured using cRMSD from its starting structure. All cRMSDs are calculated every 1 ps after superimposition on the backbone of the starting structures. Average cRMSD is calculated on 300 conformations, from 701 ps to 1 ns. The average cRMSD of the whole structure is shown in red, and that of the lipid-exchange loop is shown in blue. In the open conformation (**A**), mutations near the N- and C-termini of the lipid-exchange loop result in a decreased flexibility while mutations at middle positions of the lipid-exchange loop do not affect its flexibility. On the other hand, in the closed conformation (**B**), mutations in the middle position of the lipid-exchange loop promote its fluctuation from its starting conformations, while mutations near the N- and C- termini of the lipid-exchange loop do not alter its flexibility significantly.

energy barrier between them. To overcome this, interactions with other helper proteins may be necessary. The overall results of MD simulations imply that the open conformation is functionally relevant for the association and dissociation of retinoid to CRALBP, while the closed conformation may serve as a relatively stable carrier of retinoid, protecting them from the cellular hydrophilic environment.

All the CRAL-TRIO family members are cytosolic proteins. Both ATTP and CRALBP participate in the intracellular transfer of lipidlike ligands. The crystallographic study of ATTP has shown that the surrounding regions of the lipid-exchange loop are quite hydrophobic and facilitate docking to the membrane. Thus, interactions with the membrane lipids may be a factor to the opening of the lipid-exchange loop. Interestingly, CRALBP recently is believed to interact with ERM-binding EBP50, known as a membrane-associated protein.[7,8] This suggests that the mechanism of the lipid-exchange loop may involve membrane association.[7,8] Furthermore, the three conserved residues of CRAL-TRIO family[18] RAR (CRALBP residues 100–102), located on the top of the cleft created by the opening of the ligand-exchange loop, may play a role in regulation of the opening and the closure of the ligand–cavity entrance.

Hinge Region of the Mobile Lipid-Exchange Loop

We further investigated the hinge mechanism of the lipid-exchange loop by introducing 12 mutations in 10 residues within this loop in both the open and closed conformations: Q242R, P243A, W244A, W244F, K254A, K254Q, P255A, F256A, L257P, E263D, R264A, and V265A. MD simulations of these mutations suggest possible conservation of structural dynamics during the evolution of the CRAL-TRIO ligand-binding protein family.

In the open conformation of CRALBP, mutations near the N- and C-termini of the lipid-exchange loop result in decreased flexibility as measured by cRMSD from its starting conformation. Mutations at middle positions of the lipid-exchange loop do not affect its mobility. On the other hand, in the closed conformation, mutations in the middle position of the lipid-exchange loop promote its fluctuation from its starting conformations, while mutations near the N- and C- termini of the lipid-exchange loop do not alter its flexibility significantly (Fig. 6).

We conclude that residues Q242, P243, W244, E263, R264, and V265 are crucial for the movement of the lipid-exchange loop in its open conformation, which we call "hinge regions." Residues W244, K254, and F256 are important for keeping the lipid-exchange loop stable in its closed conformation. By mapping these residues to the sequence alignment of CRALBP with other CRAL-TRIO family members, we have found that the residues identified as essential components of the lipid-exchange loop are conserved in the CRAL-TRIO family. They are distributed in three clusters, Q242-F246, K254-L256, and E263-V265, which are conserved in CRAL-TRIO family (Fig. 1). Mutations in the structural conserved regions may affect retinoid binding, thus impairing the function of CRALBP.

CONCLUSIONS

In summary, using homology modeling methods, we have produced 3D models of open and closed conformations of human CRALBP bound to its physiological ligand, 11-*cis*-retinal. The mapping of the pathology-associated mutations (G145D, R150Q, R150W, I200T, M225K, and R233W) rationalizes the molecular basis of the impaired function of ligand binding to CRALBP that leads to retinitis pigmentosa and supports our overall model. Not all pathology-associated mutations are located inside the ligand-binding cavity, supporting the idea that mutations that change the structural integrity of the ligand-binding cavity affect the binding of retinoid to, or release from, CRALBP. Through interaction energy calculations and structural comparisons with wild-type CRALBP, we have proposed novel insights into the potential functional effects of these mutations.

Using the CRALBP closed conformation model, we have investigated 10 residues biochemically implicated in ligand binding (W165, Y179, F197, C198, M208, Q210, M222, V223, M225, and W244). Residues M208 and W244 are not involved in direct interaction with retinoid, but align at the entrance of the ligand-binding cavity, controlling the opening and the closure of the cavity. Residues Y197, Y179, M222, M225, and W165 interact with 11-*cis*-retinal directly.

Using MD simulations, we have found that in the open conformation of CRALBP, the lipid-exchange loop undergoes a dynamic process resulting in the transient unwinding of the lipid-exchange loop and subsequent binding of ligands. This is consistent with the ligand-dependent conformational changes observed in CRALBP by NMR.[16,17] Therefore, we propose functional assignments of the open and the closed conformations of CRALBP: The open conformation of CRALBP participates in the ligand association and dissociation processes; the closed form serves as a relatively stable carrier of retinoids, protecting them from the cellular hydrophilic environment.

MD simulations of a series of CRALBP mutants allowed us to identify residues essential to the flexibility of the lipid-exchange loop. These residue clusters suggest conservation of structural dynamics in the evolution of the CRAL-TRIO ligand-binding protein family. Identification of these critical residues in CRALBP contributes further structure–function studies that may guide future therapeutic efforts in recessive progressive retinopathy.

ACKNOWLEDGMENTS

We thank Aaron Chang, Gong Cheng, Kai Wang, Ling-Hong Hung, Michal Guerquin and Zach Frazier and other members of the Samudrala group for helpful comments.

REFERENCES

1. Saari JC, Sporn MB, Roberts AB, Goodman DS. The retinoids: biology, chemistry, and medicine. 2nd ed. New York: Raven Press; 1994.
2. Saari JC, Nawrot M, Kennedy BN, Garwin GG, Hurley JB, Huang J, Possin DE, Crabb JW. Visual cycle impairment in cellular retinaldehyde binding protein (CRALBP) knockout mice results in delayed dark adaptation. Neuron 2001;29:739–748.
3. Saari JC, Bredberg DL. Photocheimistry and stereoselectivity of cellular retinaldehyde-binding protein from bovine retina. J Biol Chem 1987;262:7618–7622.
4. Golovleva I, Bhattacharya S, Wu Z, Shaw N, Yang Y, Andrabi K, West KA, Burstedt MS, Forsman K, Holmgren G, Sandgren O, Noy N, Qin J, Crabb JW. Disease-causing mutations in the cellular retinaldehyde binding protein tighten and abolish ligand interactions. J Biol Chem 2003;278:12397–12402
5. Saari JC, Bredberg DL, Noy N. Control of substrate flow at a branch in the visual cycle. Biochemistry 1999;33:3106–3112.
6. Stecher H, Gelb MH, Saari JC, Palczewski K. Preferential release of 11-*cis*-retinol from retinal pigment epithelial cells in the presence of cellular retinaldehyde-binding protein. J Biol Chem 1999;274:8577–8585.
7. Nawrot M, West K, Huang J, Possin DE, Bretscher A, Crabb JW, Saari JC. Cellular retinaldehyde-binding protein interacts with ERM-binding phosphoprotein 50 in retinal pigment epithelium. Investig Ophthalmol Vis Sci 2004;45:393–401.
8. Bonilha VL, Bhattacharya SK, West KA, Crabb JS, Sun J, Rayborn ME, Nawrot M, Saari JC, Crabb JW. Support for a proposed retinoid-processing protein complex in apical retinal pigment epithelium. Exp Eye Res 2004;79:419–422.
9. Demirci FY, Rigatti BW, Mah TS, Gorin MB. A novel compound heterozygous mutation in the cellular retinaldehyde-binding protein gene (RLBP1) in a patient with retinitis punctata albescens. Am J Ophthalmol 2004;138:171–173.
10. Maw MA, Kennedy B, Knight A, Bridges R, Roth KE, Mani EJ, Mukkadan JK, Nancarrow D, Crabb JW, Denton MJ. Mutation of the gene encoding cellular retinaldehyde-binding protein in autosomal recessive retinitis pigmentosa. Nat Genet 1997;17:198–200.
11. Burstedt MS, Sandgren O, Holmgren G, Forsman-Semb K. Bothnia dystrophy caused by mutations in the cellular retinaldehyde-binding protein gene (RLBP1) on chromosome 15q26. Invest Ophthalmol Vis Sci 1999;40:995–1000.
12. Morimura H, Berson EL, Dryja TP. Recessive mutations in the RLBP1 gene encoding cellular retinaldehyde-binding protein in a form of retinitis punctata albescens. Invest Ophthalmol Vis Sci 1999;40:1000–1004.
13. Eichers ER, Green JS, Stockton DW. Newfoundland rod-cone dystrophy, an early-onset retinal dystrophy, is caused by splice-junction mutations in RLBP1. Am J Hum Genet 2002;70:955–964.
14. Fishman GA, Roberts MF, Derlacki DJ. Novel mutations in the cellular retinaldehyde-binding protein gene (RLBP1) associated with retinitis punctata albescens: evidence of interfamilial genetic heterogeneity and fundus changes in heterozygotes. Arch Ophthalmol 2004;122:70–75.
15. Crabb JW, Nie Z, Chen Y, Hulmes JD, West KA, Kapron JT, Ruuska SE, Noy N, Saari JC. Cellular retinaldehyde-binding protein ligand interactions. J Biol Chem 1998;273:20712–20720.
16. Wu Z, Yang Y, Shaw N, Bhattachary S, Yan L, West K, Roth K, Noy N, Qin J, Crabb JW. Mapping the ligand binding pocket in the cellular retinaldehyde binding protein. J Biol Chem 2003;278:12390–12396.
17. Wu Z, Hasan A, Liu T, Teller DC, Crabb JW. Identification of CRALBP ligand interactions by photoaffinity labeling, hydrogen/

deuterium exchange, and structural modeling. J Biol Chem 2004;279:27357–27364.
18. Panagabko C, Morley S, Hernandez M, Cassolato P, Gordon H, Parsons R, Manor D, Atkinson J. Ligand specificity in the CRAL-TRIO protein family. Biochemistry 2003;42:6467–6474.
19. Meier R, Tomizaki T, Schulze-Briese C, Baumann U, Stocker A. The molecular basis of vitamin E retention: structure of human alpha-tocopherol transfer protein. J Mol Biol 2003;331:725–734.
20. Min KC, Kovall RA, Hendrickson WA. Crystal structure of human α-tocopherol transfer protein bound to its ligand: implications for ataxia with vitamin E deficiency. Proc Natl Acad Sci USA 2003;100:14713–14718.
21. Sha B, Phillips SE, Bankaitis VA, Luo M. Crystal structure of the *Saccharomyces cerevisiae* phosphatidylinositol-transfer protein. Nature 1998;391:506–510.
22. Stocker A, Baumann U. Supernatant protein factor in complex with RRR-alpha-tocopherylquinone: a link between oxidized vitamin E and cholesterol biosynthesis. J Mol Biol 2003;332:759–765.
23. Samudrala R, Moult J. An all-atom distance-dependent conditional probability discriminatory function for protein structure prediction. J Mol Biol 1998;275:893–914.
24. Samudrala R, Moult J. A graph-theoretic algorithm for comparative modelling of protein structure. J Mol Biol 1998;279:287–302.
25. Canutescu AA, Shelenkov AA, Dunbrack RL. A graph theory algorithm for protein side-chain prediction. Protein Sci 2003;12: 2001–2014.
26. Levitt M, Hirshberg M, Sharon R, Daggett V. Potential energy function and parameters for simulations of the molecular dynamics of proteins and nucleic acids in solution. Comp Phys Comm 1995;91:215–231.
27. Kalé L, Skeel R, Bhandarkar M, Brunner R, Gursoy A, Krawetz N, Phillips J, Shinozaki A, Varadarajan K, Schulten K. NAMD2: greater scalability for parallel molecular dynamics. J Comp Phys 1999;151:283–312.
28. Brooks BR, Bruccoleri RE, Olafson BD, States DJ, Swaminathan S, Karplus M. CHARMM: a program for macromolecular energy, minimization, and dynamics calculations. J Comp Chem 1983;4: 187–217.
29. MacKerell AD, Brooks BR, Brooks CR, Nilsson IL, Roux B, Won Y, Karplus M. CHARMM: the energy function and its parameterization with an overview of the program. In: Schleyer PR, editor. Encyclopedia of computational chemistry. Chichester, UK: Wiley; 1998. p 271–277.
30. Laskowski RA, MacArthur MW, Moss DS, Thornton JM. PROCHECK: a program to check the stereochemical quality of protein structures. J Appl Crystallogr 1993;26:283–291.
31. Kraulis P. MOLSCRIPT: a program to produce both detailed and schematic plots of protein structures. J Appl Crystallogr 1991;24: 946–950.
32. Merritt E, Bacon DJ. Raster3D: photorealistic molecular graphics. Methods Enzymol 1997;277:505–524.
33. Brunger AT. X-PLOR version 3.1, a system for X-ray crystallography and NMR. New Haven, CT: Yale University Press; 1992.
34. Kleywegt GJ, Jones TA. Databases in protein crystallography. Acta Crystallogr D Biol Crystallogr 1998;54:1119–1131.
35. NAMD Wiki: ParameterTopologyRepository. http://www.ks.uiuc.edu/Research/namd/wiki/index.cgi?ParameterTopology Repository
36. Humphrey W, Dalke A, Schulten K. VMD—visual molecular dynamics. J Mol Graphics 1996;14:33–38.
37. Grubmüller H, Heymann B, Tavan P. Ligand binding: Molecular mechanics calculation of the streptavidin–biotin rupture force. Science 1996;271:997–999.
38. Martyna GJ, Tobias DJ, Klein ML. Constant pressure molecular dynamics algorithms. J Chem Phys 1994;101:4177–4189.